International Forum on Aeroelasticity and Structural Dynamics
IFASD 2024
17-21 June 2024, The Hague, The Netherlands

INVESTIGATING MULTI–BODY FLIGHT DYNAMIC MODES OF AN AIRCRAFT WITH SEMI-AEROELASTIC HINGE

A.H Modarres[1], V. Maltsev[1], Z. Li[1], D. Clifford[1], A. Da Ronch[1]

[1]University of Southampton
School of Engineering, SO16 3BE Southampton, United Kingdom
A.H.Modarres-Aval@soton.ac.uk

Keywords: Multi-Body-Dynamics, Aeroelasticity, Semi-aeroelastic hinge

Abstract:

The aerodynamic efficiency of an aircraft can be improved by adopting wings with a very high aspect ratio. However, the limitation to the wing size imposed by airport regulation and the increased structural weight required to support the extra aerodynamic loads produced by high aspect ratio wings need to be carefully addressed. To solve these issues, the concept of aircraft with semi-aeroelastic hinges which enables floating wingtips has been recently proposed and has attracted the attention of many researchers. However, this study provides new insights into this idea from the aspect of constraint loads at the hinges. In this work, using a multi–body dynamic simulation and a nonlinear quasi–steady aerodynamic model, an aircraft with articulated wings has been mathematically modelled, with the aircraft being composed of three rigid parts. This multi–body formulation enables one to account for finite rotations of rigid folding wing tips in addition to the traditional flight dynamic modes. Despite having a relatively small folded wing tip mass in the case study investigated here some changes have been observed in the flight dynamic behavior of the aircraft. A systematic study was carried out for different values of hinge flare angle and wingtip mass. It was found that the amount of forces and moments acting at the hinges is quite considerable and should be carefully accounted for during the preliminary design stage. In the presence of a side-slip angle, the asymmetric transient forces and moments at hinges can lead to larger deviation from the initial flight path.

1 INTRODUCTION

In order to reduce the lift induced drag, which is a great contributor to the overall drag, modern aircraft tend to have very high aspect ratio wings. The folding wing tip (FWT) [1, 2] concept is introduced to solve two issues related to high aspect ratio wings: on the ground, the wingspan is reduced to meet the airport gate size limits, while in flight, it can be used as load alleviation device. The FWT device allows the rotation of the wingtips around a hinge axis which is typically not aligned with the oncoming flow, but rotated outboard of the streamline by the so-called flare angle. In the semi aeroelastic hinge approach (SAH) [3], while cruising, the wingtip is locked in such a way to maximize the wingspan, and is released when encountering triggering events such as wind gust. When the wingtip is allowed to rotate, the fold angle, defined as the angle between the planes cutting main wing and wingtip, tends to an equilibrium position reaching a coasting angle, where aerodynamic and inertial forces balance each other. Previous studies [1–3] investigated the effect of flare angle, wing tip mass, hinge stiffness, and hinge location on the coast angle.

Castrichini et al. [2] showed that the effect of the flare angle is to reduce the local angle of attack of the wingtip when it rotates around the hinge axis, decreasing the loads acting on the wing. Castrichini [2] and Ye. [4] investigated the effect of hinge stiffness and flare angle on the bending moment, finding, as expected, that for non–zero flare angles, the bending moment decreases with the stiffness of the hinge since larger deflection are achieved for the wingtips and thus lower local angle of attack. Generally, for moderate flare angles, small hinge stiffness and wingtip mass, the FWT device has beneficial load alleviation effect. However, as discussed in [5], the use of zero stiffness hinge can lead to flutter which has to be corrected using tip masses. Castrichini [6] evaluated the effect on load alleviation for different timing between SAH release and gust encounter, finding that a prompt release of the wingtip is necessary to be effective. Leylek and Costello [7] showed that the introduction of an elastic hinge on the wing causes flexible modes and low-order dynamics modes coupling, affecting the flight dynamic response of the vehicle, and also having non–zero flare angle for the hinge axis introduces lateral and longitudinal wing motions coupling.

This work herein is part of a recent effort led by Airbus in the frame of the Out of cycle NExt generation highly efficient air transport (ONEheart) project and us as a research group at the University of Southampton develop technology bricks to enable overall aircraft design. In this study, we investigate how flight modes and handling qualities of the vehicle are affected by the added flexibility to the wing. A representative civil jet aircraft with articulated wings is used to explore the effect of introducing a wing-tip device, connected to the wings with an elastic hinge, on the flight dynamic modes of the vehicle. The articulated aircraft is modelled as a multi–body problem and is composed of three rigid parts. For the aerodynamic loads evaluation a nonlinear quasi steady representation is adopted and the framework is used to study the flight dynamic behaviour for finite rotation of the FWT device. The effects of different structural-hinge elastic properties, orientation, wing tip weight on the dynamics and on the time history of the constraint forces and moments on the hinge in different flight regimes are examined.

The orientations of the hinges are symmetrical to the x-z plane of the aircraft. However, side–slip can easily cause an asymmetry in the hinge orientation which may have an important effect on the flight dynamic response of the vehicle, therefore one of our primary goals in this study is to investigate the side–slip effect. Therefore, the asymmetry on the fold angle due to initial slideslip and the effect on the flight dynamic response is also examined.

Despite the interest on the topic of SAH, there are only a few studies which consider the effect of multi–body dynamics on the folded wing tip response. The main novelty of the current study is to adopt a set of equations governing the multi–body dynamic behaviour of the system to analyze the FWTs response. In addition, for the derivation of the equations, the whole system is treated as three decoupled rigid bodies and equilibrium equations are written for each body individually. This approach enables us to compute the wingtips local angle of attack exactly, considering the contributions due to all rotational and transformational velocities, and to monitor the transient and steady–state constraints loads at the hinges which are crucial for the design of the hinge and any desirable controller and actuator. The current strategy to tackle the problem also enables us also to investigate the different responses of the left and right FWTs in presence of a side–slip angle. A similar treatment of the problem has not been considered among studies regarding the SAH concept.

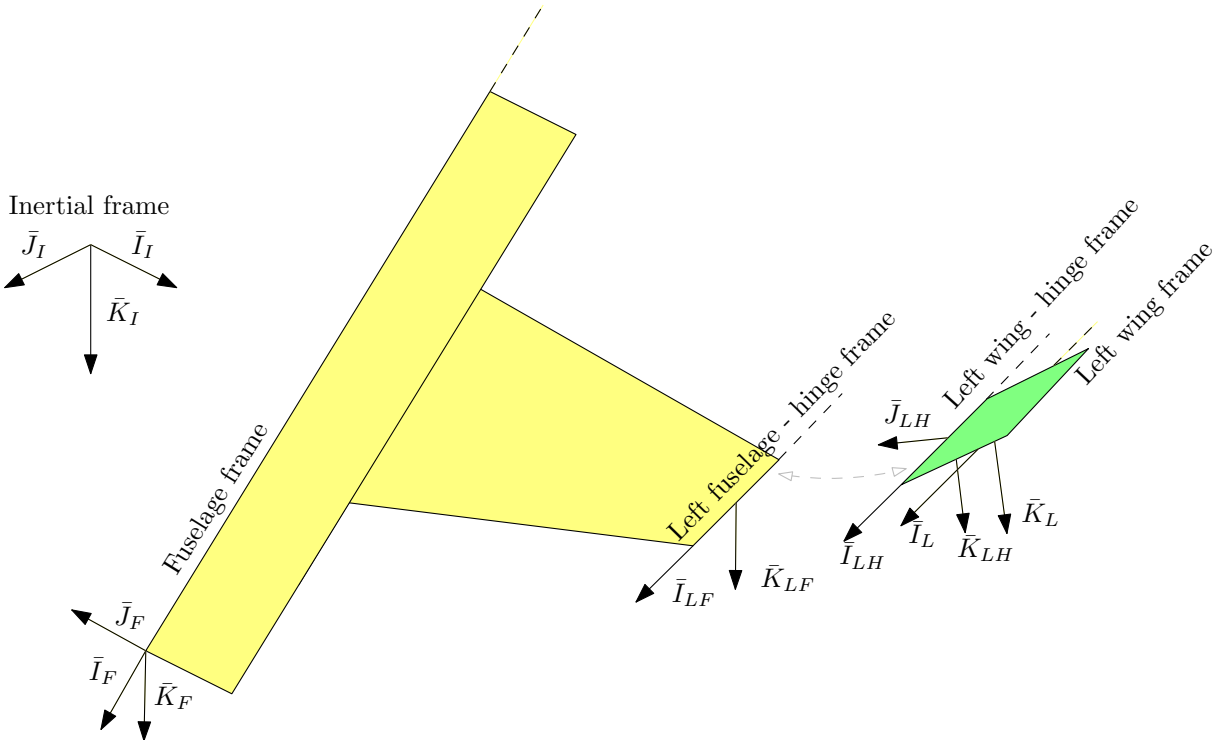

Figure 1: Schematic of the various reference frames

2 METHODOLOGY

At the extremes of the main wings, the wingtips are connected to the wing-fuselage frame through a revolute joint. This results in the addition of two degrees of freedom (DOF) to the conventional six-DOF rigid-body aircraft model. This multi-body-dynamic system is overall composed of three rigid bodies, including the fuselage and main central wings, left FWT, and right FWT, with a total of eight DOF. Each body has a body reference frame with the origin located at the body's center of gravity (c.g.). A frame aligned with the hinge axis is also defined at the joint on each body.

In Figure 1, a schematic depicting the dynamic system is illustrated. The transformation between the inertial frame and the body frame of the fuselage is given as:

$$\begin{bmatrix} \bar{\mathbf{I}}_F \\ \bar{\mathbf{J}}_F \\ \bar{\mathbf{K}}_F \end{bmatrix} = [T_{FI}] \begin{bmatrix} \bar{\mathbf{I}}_I \\ \bar{\mathbf{J}}_I \\ \bar{\mathbf{K}}_I \end{bmatrix}, \tag{1}$$

where the transformation matrix $[T_{FI}]$, defined as in Equation 2, is based on Euler angles. Equations 3-5 represent the rotations between the body frames of the system, from fuselage to left fuselage, from left fuselage to left hinge and from left hinge to left folding wing tip respectively. The rotation matrix T_β is the rotation of the wing around the joint axis represented by the fold angle β_L, as described in Equation 6.

$$[T_{FI}] = \begin{bmatrix} \cos\theta\cos\psi & \cos\theta\sin\psi & -\sin\theta \\ \sin\phi\sin\theta\cos\psi - \cos\theta\sin\psi & \sin\phi\sin\theta\sin\psi + \cos\theta\cos\psi & \sin\phi\cos\theta \\ \cos\phi\sin\theta\cos\psi + \sin\phi\sin\psi & \cos\phi\sin\theta\sin\psi - \sin\theta\cos\psi & \cos\phi\cos\theta \end{bmatrix}, \tag{2}$$

$$\begin{bmatrix} \bar{\mathbf{I}}_{LF} \\ \bar{\mathbf{J}}_{LF} \\ \bar{\mathbf{K}}_{LF} \end{bmatrix} = [T_{LF}] \begin{bmatrix} \bar{\mathbf{I}}_{F} \\ \bar{\mathbf{J}}_{F} \\ \bar{\mathbf{K}}_{F} \end{bmatrix}, \tag{3}$$

$$\begin{bmatrix} \bar{\mathbf{I}}_{LH} \\ \bar{\mathbf{J}}_{LH} \\ \bar{\mathbf{K}}_{LH} \end{bmatrix} = [T_{\beta_L}] \begin{bmatrix} \bar{\mathbf{I}}_{LF} \\ \bar{\mathbf{J}}_{LF} \\ \bar{\mathbf{K}}_{LF} \end{bmatrix}, \tag{4}$$

$$\begin{bmatrix} \bar{\mathbf{I}}_{L} \\ \bar{\mathbf{J}}_{L} \\ \bar{\mathbf{K}}_{L} \end{bmatrix} = [T_{LH}] \begin{bmatrix} \bar{\mathbf{I}}_{LH} \\ \bar{\mathbf{J}}_{LH} \\ \bar{\mathbf{K}}_{LH} \end{bmatrix}, \tag{5}$$

$$[T_{\beta_L}] = \begin{bmatrix} 1 & 0 & 0 \\ 0 & \cos(\beta_L) & \sin(\beta_L) \\ 0 & -\sin(\beta_L) & \cos(\beta_L) \end{bmatrix}. \tag{6}$$

For the derivation of the equations, each part was treated as a decoupled rigid body and equilibrium equations were written for each of them individually. This ends up having a total of eighteen equations. In addition, Euler kinematic equations have been utilized to connect body axis rotation to Euler angles. The final equations of motion can be presented in a matrix form as follows:

$$Ax = B, \tag{7}$$

where the matrix A is defined as:

$$A = \begin{bmatrix} m_f I_{33} & 0_{33} & 0_{31} & 0_{31} & -I_{33} & -I_{33} & 0_{32} & 0_{32} \\ 0_{33} & I_F & 0_{31} & 0_{31} & -S_L & -S_R & -T_{LF}^T \Phi_L & -T_{RF}^T \Phi_R \\ m_L T_L & -m_L(T_L S_L - S_{LL} T_L) & -m_L S_{LL} T_{LH}^T \Lambda_L & 0_{31} & T_L & 0_{33} & 0_{32} & 0_{32} \\ 0_{33} & I_L T_L & I_L T_{LH}^T \Lambda_L & 0_{31} & S_{LL} T_L & 0_{33} & T_{LH}^T T_{\beta_L} \Phi_L & 0_{32} \\ m_R T_R & -m_R(T_R S_R - S_{RR} T_R) & 0_{31} & -m_R S_{RR} T_{RH}^T \Lambda_R & 0_{33} & T_R & 0_{32} & 0_{32} \\ 0_{33} & I_R T_R & 0_{31} & I_R T_{RH}^T \Lambda_R & 0_{33} & S_{RR} T_R & 0_{32} & T_{RH}^T T_{\beta_R} \Phi_R \end{bmatrix}, \tag{8}$$

and the vector B includes the right hand side of the system, which in expanded form writes:

Property:	Main wing	Tail wing	FWTs
Planform area (m^2)	260	64	18
mass (kg)	(120000 *aircraft total*)		1000
mean chord $\bar{c}$ (m)	6.6	-	6.6
dihedral (deg)	5	-	-

Table 1: Geometrical features of main wing, tail wing and FWTs

$$B_1 = -m_{_F} S_{\omega_{_F}} \vec{V}^{F}_{F} + \vec{F}^{F}_{F_{Aero}} + \vec{F}^{F}_{F_{Grav}} + \vec{F}^{F}_{Thrust}, \tag{9}$$

$$B_2 = -S_{\omega_{_F}} I_{_F} \vec{\omega}^{F}_{F} - T^{T}_{LF} \Lambda_{_L} M_{L_{elastic}} - T^{T}_{RF} \Lambda_{_R} M_{R_{elastic}} + \vec{M}^{F}_{F_{Aero}} + \vec{M}^{F}_{Torque} \tag{10}$$

$$B_3 = -m_{_L} T_{_L} \left(S_{\omega_{_F}} \vec{V}^{F}_{F} + S_{\omega_{_F}} S_{\omega_{_F}} \vec{r}^{F}_{L} \right) + m_{_L} S_{LL} T^{T}_{LH} \dot{T}_{\beta_{_L}} T_{LF} \vec{\omega}^{F}_{F} - m_{_L} S_{\omega^{L}_{L}} S_{\omega^{L}_{L}} \vec{r}^{L}_{LL} + \vec{F}^{L}_{L_{Aero}} + \vec{F}^{L}_{L_{Grav}}, \tag{11}$$

$$B_4 = -I_{_L} T^{T}_{LH} \dot{T}_{\beta_{_L}} T_{LF} \vec{\omega}^{F}_{F} - S_{\omega^{L}_{L}} I_{_L} \vec{\omega}^{L}_{L} + T^{T}_{LH} T_{\beta_{_L}} \Lambda_{_L} M_{L_{elastic}} + \vec{M}^{L}_{L_{Aero}}, \tag{12}$$

$$B_5 = -m_{_R} T_{_R} \left(S_{\omega_{_F}} \vec{V}^{F}_{F} + S_{\omega_{_F}} S_{\omega_{_F}} \vec{r}^{F}_{R} \right) + m_{_R} S_{RR} T^{T}_{RH} \dot{T}_{\beta_{_R}} T_{RF} \vec{\omega}^{F}_{F} - m_{_R} S_{\omega^{R}_{R}} S_{\omega^{R}_{R}} \vec{r}^{R}_{RR} + \vec{F}^{R}_{R_{Aero}} + \vec{F}^{R}_{R_{Grav}}, \tag{13}$$

$$B_6 = -I_{_R} T^{T}_{RH} \dot{T}_{\beta_{_R}} T_{RF} \vec{\omega}^{F}_{F} - S_{\omega^{R}_{R}} I_{_R} \vec{\omega}^{R}_{R} + T^{T}_{RH} T_{\beta_{_R}} \Lambda_{_R} M_{R_{elastic}} + \vec{M}^{R}_{R_{Aero}}. \tag{14}$$

The system is then solved for the vector of unknowns x which includes the time derivative of the velocity, angular velocity, angular acceleration of the folding wingtip and the constraint loads (forces and moments).

$$x = \begin{bmatrix} \dot{\vec{V}}_{F} & \dot{\vec{\omega}}_{F} & \ddot{\beta}_{_L} & \ddot{\beta}_{_R} & \vec{F}_{LH} & \vec{F}_{RH} & M_{LH} & M_{RH} \end{bmatrix}^{T}. \tag{15}$$

3 RESULTS

Case study: As a form of verification of the present study, the free response of the system to a set of initial conditions is evaluated assigning increasingly larger values for the mass of the FWTs. The test case is set up building on the standard RCAM model [8], using the parameters defined in Table 1 and Table 2. The inertia matrices used in Equations 3-5 are computed using the aforementioned geometric parameters and are represented in Equation 16, where the total aircraft mass is equal to 120 tons. Herein, the directions X, Y, Z refer to directions $\bar{I}_F, \bar{J}_F, \bar{K}_F$ respectively, of the fuselage body frame defined in Figure 1.

Figure 2 represents the time history of the four nonzero state variables when longitudinal modes are excited. It can be observed that as the mass of folding wing tips decreases, the multi–body

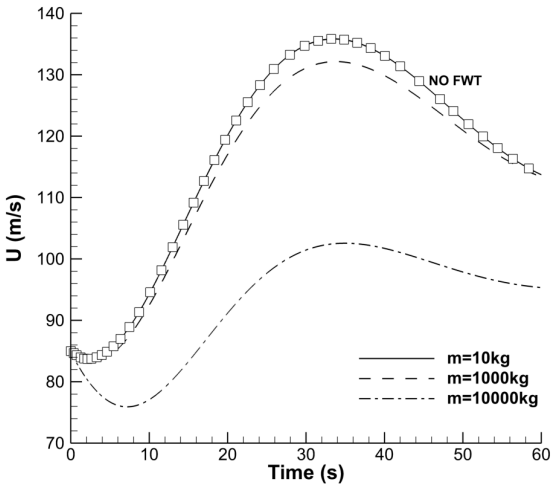

(a) velocity in X_F direction

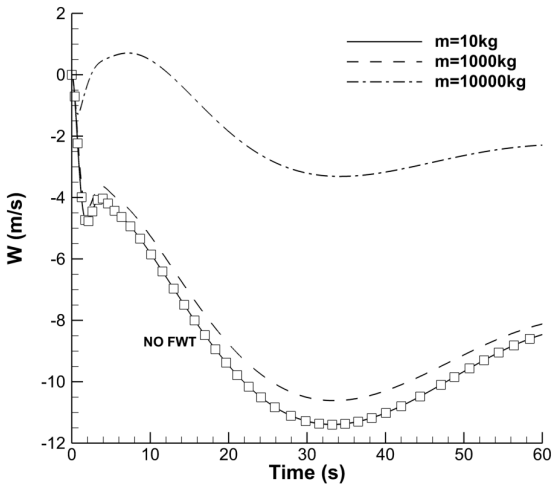

(b) velocity in Z_F direction

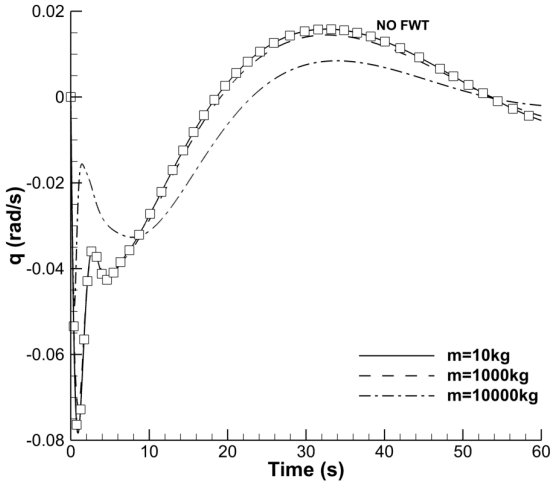

(c) body axis pitch rate

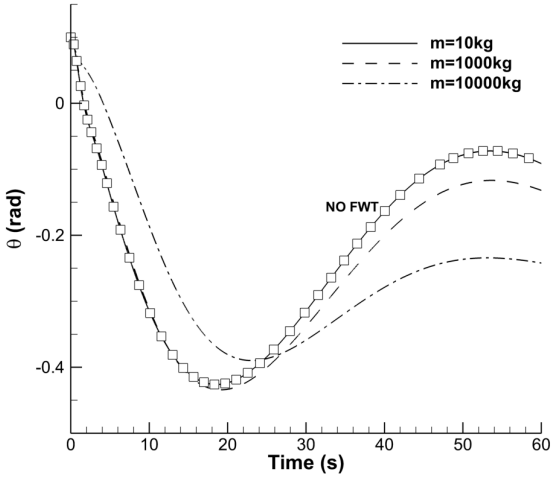

(d) Euler pitch angle

Figure 2: State variables response in time

dynamic response converges to the RCAM model response, referred to as a rigid model in the figure label. Also, it can be seen that for the parameters being chosen here, the effect on the system response of FWTs becomes more appreciable for FWTs masses larger than 100kg, and a value of 1000kg is assumed for the wingtips mass in the following test cases.

$$I_F = m \begin{bmatrix} 40.07 & 0.0 & -2.09 \\ 0.0 & 64 & 0.0 \\ -2.09 & 0.0 & 99.92 \end{bmatrix}, \quad I_L = m_L/S_L \begin{bmatrix} 7.15 & -2.08 & 0.0 \\ -2.08 & 2.220 & 0.0 \\ 0.0 & 0.0 & 9.35 \end{bmatrix}, \quad (16)$$
$$I_R = m_R/S_R \begin{bmatrix} 7.15 & 2.08 & 0.0 \\ 2.08 & 2.220 & 0.0 \\ 0.0 & 0.0 & 9.35 \end{bmatrix}.$$

Due to the lack of similar studies, reference values for the state variables are not available, and as an additional verification of the derivation and implementation of the current approach, the

Location:	**x coord.** (m)	**y coord.** (m)	**z. coord** (m)
Center of gravity (CoG)	$0.23\bar{c}$	0	$0.10\bar{c}$
Aerodynamic center (AC)	$0.12\bar{c}$	0	0
Engine 1 location	0	-7.94	-1.9
Engine 2 location	0	7.94	-1.9

Table 2: Location of center of gravity, ac and engines with respect to the fuselage frame body

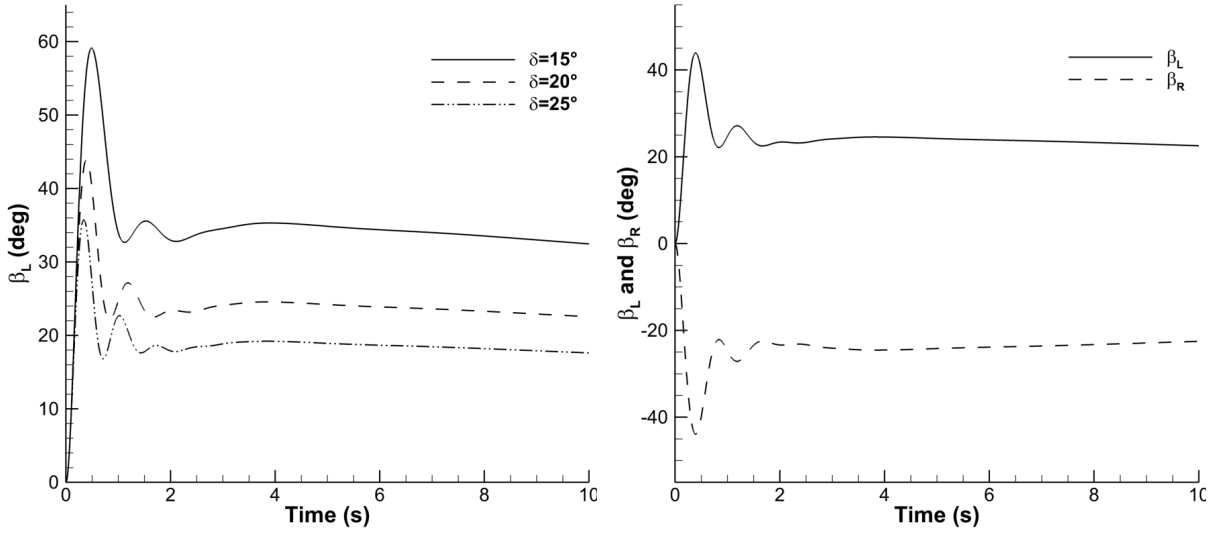

(a) Left FWT folding angle w.r.t. flare angle (b) Left and right FWTs folding angle time history

Figure 3: FWTs response in time without initial side-slip angle

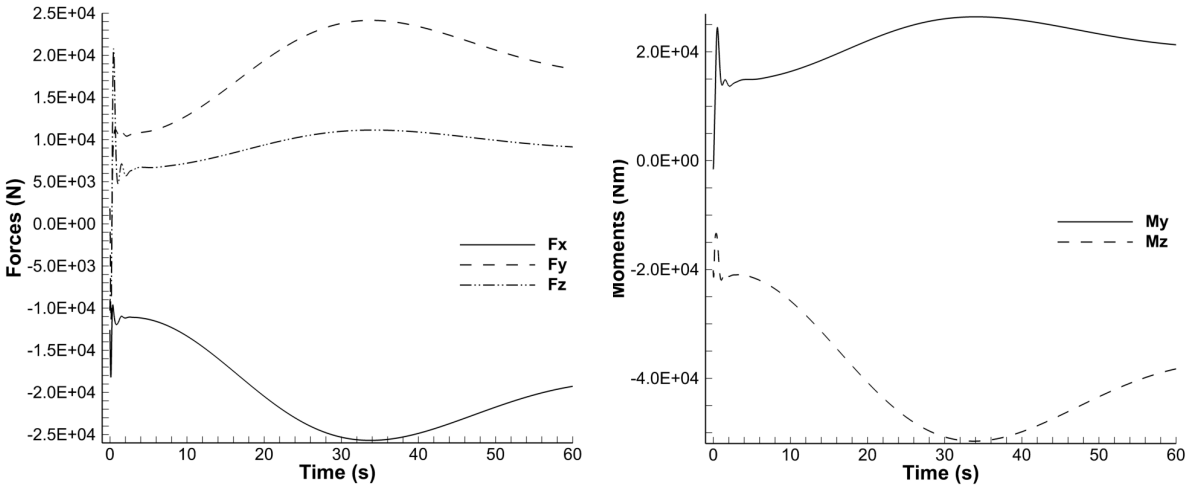

(a) Reaction forces components at the hinge (b) Reaction moments components at the hinge

Figure 4: Reaction forces at the hinge

effect of the flare angle δ on the fold angle β is monitored. The time history for the first 20 seconds of the fold angle response to the initial condition defined previously are represented in Figure 3a, for flare angles of $15°, 20°, 25°$ respectively. As can be seen from the figure, the

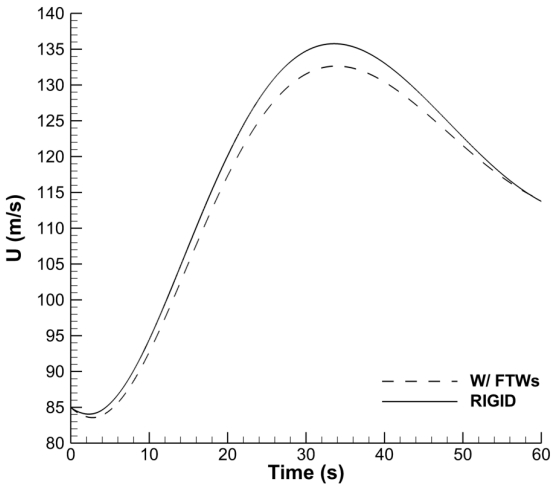

(a) velocity on X_F direction

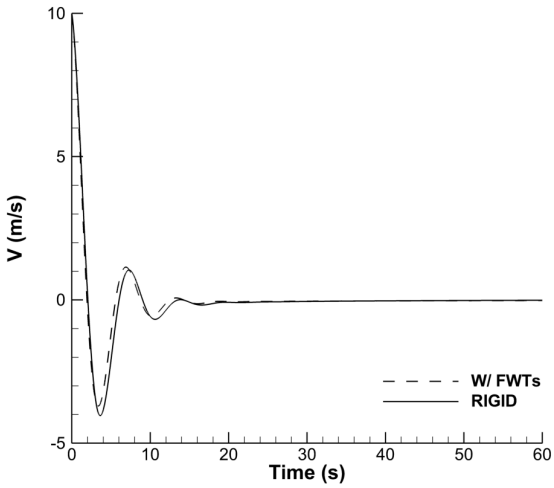

(b) velocity in Y_F direction

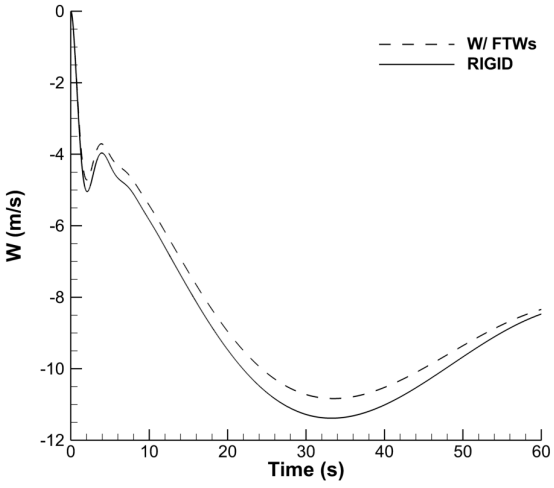

(c) velocity in Z_F direction

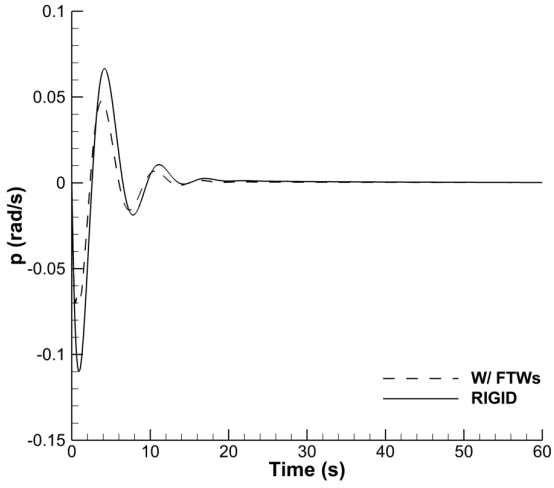

(d) body axis roll rate

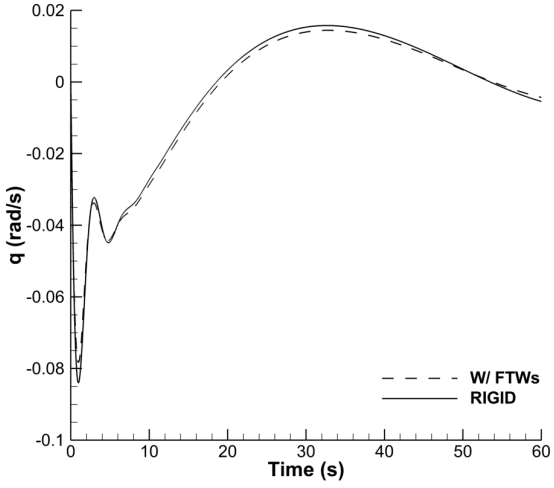

(e) body axis pitch rate

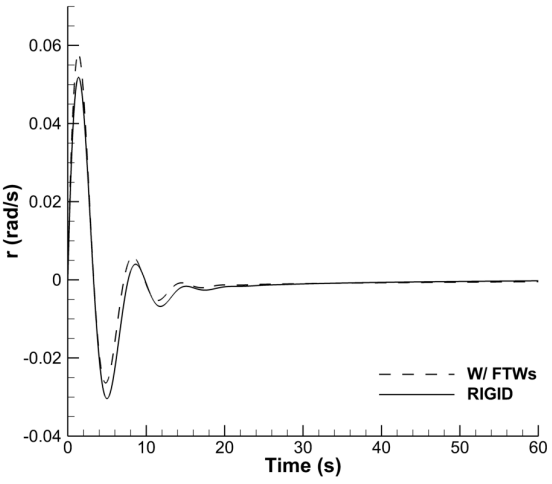

(f) body axis yaw rate

Figure 5: State variables response considering initial angle of side-slip

folded wing tips response can be divided into a transient and a steady-state response. Two peaks can be observed before the fold angle converges to an equilibrium value (coast angle) which in

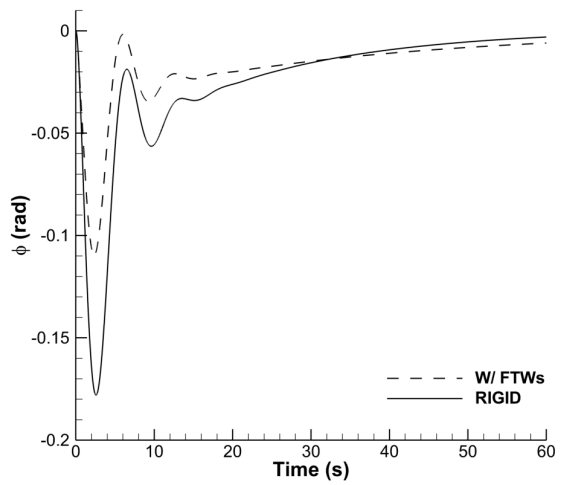

(g) Euler roll angle

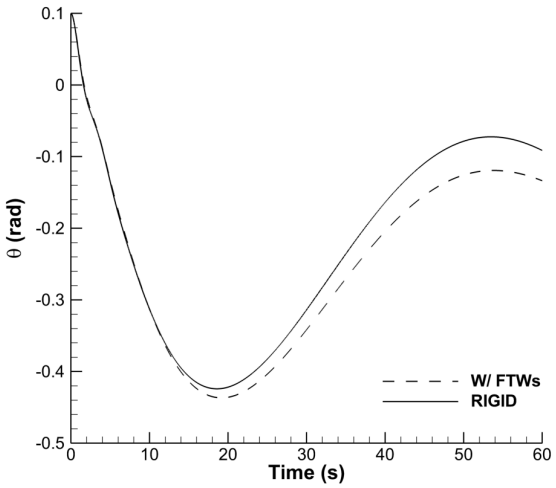

(h) Euler pitch angle

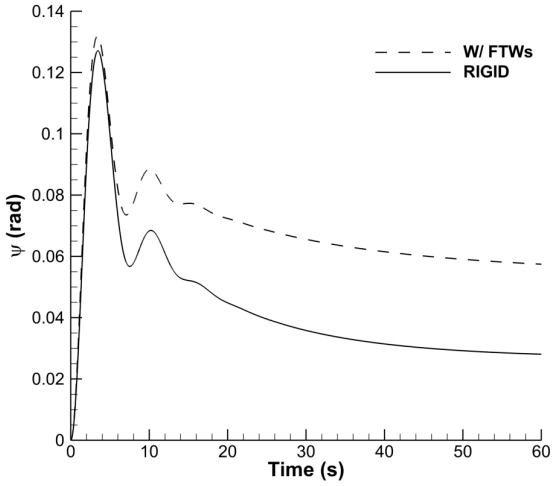

(i) Euler yaw angle

Figure 5: (*continued*) State variables response considering initial angle of side-slip

this case is almost 20 degrees, at which inertial and aerodynamic forces balance each other. Larger coasting angles and longer transient periods are found for correspondingly smaller flare angles. Both the transient and steady-state responses for the left and right FWTs are completely symmetric, as expected when there is no initial side-slip angle, as shown in Figure 3b. The reaction forces and moments acting on the fuselage at the hinge are illustrated in Figure 4. We noted that the F_y force for both left and right hinges acts on the inward directions. In the absence of the side-slip angle, the constraint forces and moments are fully symmetric. The values associated with moments components have been presented in the left and right fuselage frames. An important consideration here is that the direction of constraint force in the Z direction is upward which means that the FWTs do contribute to the total lift acting on the aircraft. As shown in Figure 4, the amount of forces and moments is quite considerable and should be carefully accounted for during the preliminary design stage. The amount of force in the negative X direction is significant, and it should be noted that this is not favourable from an efficiency standpoint.

In the next step, the state variables of the system are excited with an initial non-zero side-slip

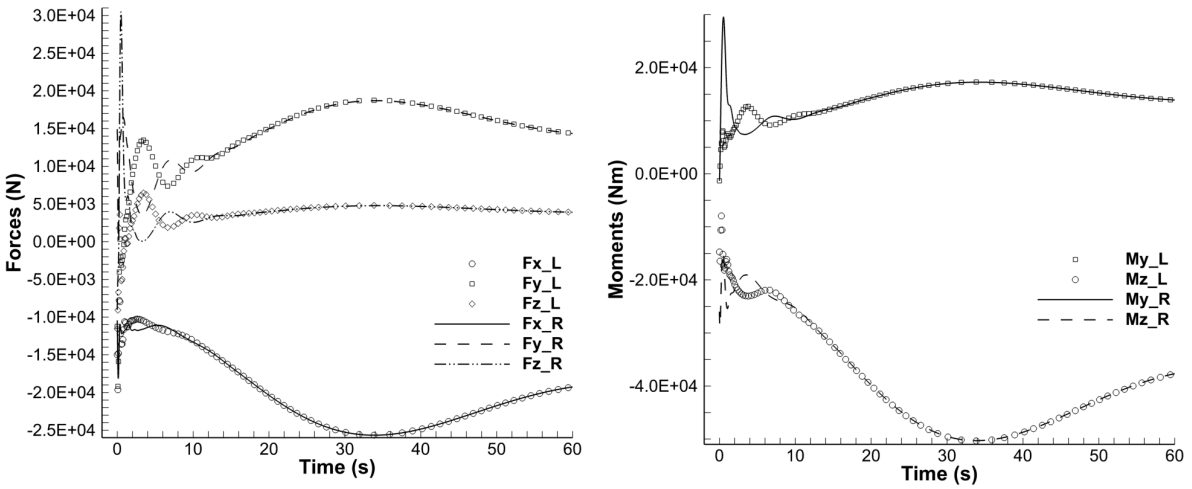

(a) Reaction forces components at the hinge (b) Reaction moments components at the hinge

Figure 6: Reaction forces at the hinge with initial side–slip

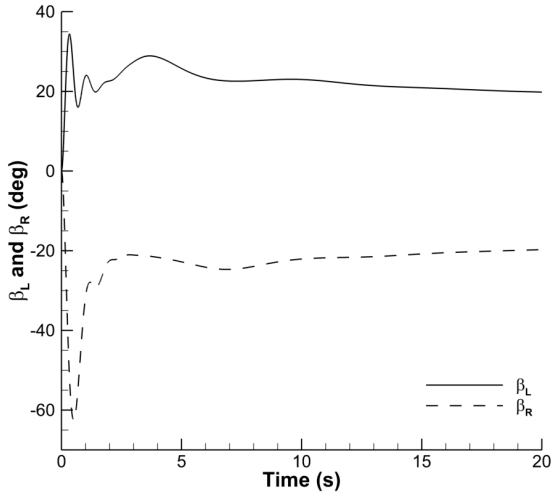

Figure 7: Left and right wing-tip folding angle, β_L and β_R with initial angle of side-slip

angle. Figure 5 indicates the time response of the first nine state variables of both standard rigid aircraft and aircraft with FWTs, where lateral modes are also represented, having here non-zero values. As the figure indicates, after almost 20 seconds, the velocity of the aircraft in the y-direction decays to zero and as a consequence also the side-slip angle goes to zero. Therefore, it can be concluded that both aircraft are stable with respect to the presence of the initial non-zero side-slip angle. In addition, it can also be demonstrated that except for Euler's pitch and yaw angle, all the other state variables converge almost to the same steady-state values. The difference in the Euler pitch angle is almost the same as the value found in absence of initial side-slip (Figure 2d) and this is mainly due to the difference in the total mass of the aircraft. The difference in Euler yaw angle value is more intriguing from the aspect of the flight path, as it implies that rigid and folded wing tip aircraft with a non-zero initial side-slip angle tend to point to different directions. To justify this steady-state gap in the direction of the flight we need to take a closer look at the forces and moments acting at the hinges, showed in figure 6. In the presence of the side-slip, these forces and moments are certainly asymmetric during the transient response of the aircraft. These asymmetric forces and moments will lead to a transient

Aircraft	u	v	w	p	q	r	ϕ	θ	ψ	β_L	β_R
Rigid	84.9905	0	1.2713	0	0	0	0	0.015	0	-	-
Rigid w/ FWTs	84.9905	0	1.2713	0	0	0	0	0.015	0	0.587	-0.587

Table 3: State variables trim conditions for rigid and rigid with FWTs aircraft. The u, v, w variables are expressed in (m/s), variables p, q, r in (rad/s) and ϕ, θ, ψ in (rad)

Input	Rigid	Rigid w/ FWTs
Aileron (rad)	0	0
Stabilizer (rad)	-0.178	-0.1732
Rudder (rad)	0	0
Engine 1	0.0821	0.0918
Engine 2	0.0821	0.0918

Table 4: Input trim conditions for rigid and rigid with FWTs aircraft

moment around the Z direction, which consequently ends up creating a yaw angle. On the other hand, since the aircraft is neutrally stable with respect to the yaw angle and there is no restoring force to put it back in the initial direction, it remains in the new direction.

Figure 7 displays the time response of left and right folded wing tip angles, β_R and β_L, in the presence of initial side-slip angle. It is apparent that the two FWTs experience different transient but same steady-state response. We can also see that in spite of having a non-zero initial side-slip angle, the side-sleep approaches zero after a quite short time. So the steady-state value of the side-slip angle is zero. On the other hand, we know that in the presence of the side-slip angle, each FWTs experiences a different flare angle and therefore their responses are also different. As we mentioned earlier, the left and right FWTs have various transients, but they both have the same steady-state response. Since by reducing the flare angle the FWT becomes more unstable, from Figure 7 it can be concluded that the right FWT has an initially larger flare angle in comparison to the left one. The same conclusion can be also supported by Figure 5.

Table 3 and Table 4 compare, respectively, the values of state variables and input of both rigid and rigid with FWTs aircraft configurations, for the same trim condition, where the steady state straight and level trimmed flight are reached at a total velocity of 85 m/s. It can be seen from Table 4 that by adding the folded wing tips to the rigid configuration, thus increasing the total mass of the whole aircraft by $\approx 2\%$, the engine level operating conditions have been increased by $\approx 10\%$. By looking at the values of constraint forces for the steady-state, straight and level-trimmed flight condition in Table 5, this increase in the level of engine operation can be justified. As can be seen, the steady-state value of the constraint forces is a relatively high

Var.	F_x (kN)	F_y (kN)	F_y (kN)	β_L (deg)	β_R (deg)
Trim value	-11.267	10	4.82	33.65	-33.65

Table 5: Constraint loads and folding angle values at trim conditions

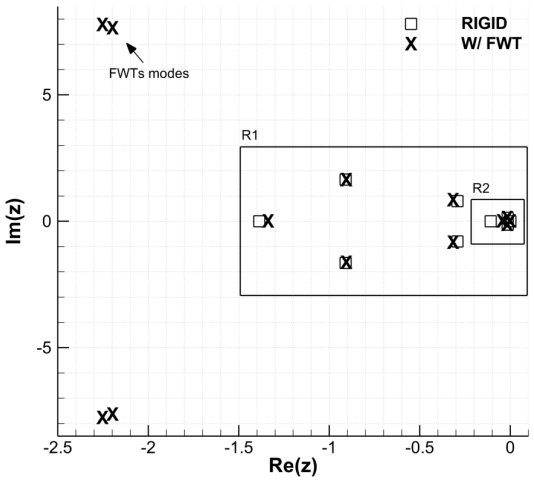

(a) Overview of complete set of flight dynamic modes root locus

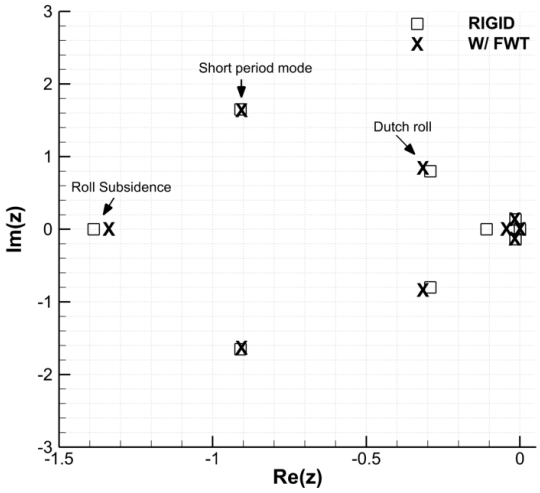

(b) Zoom on region R1

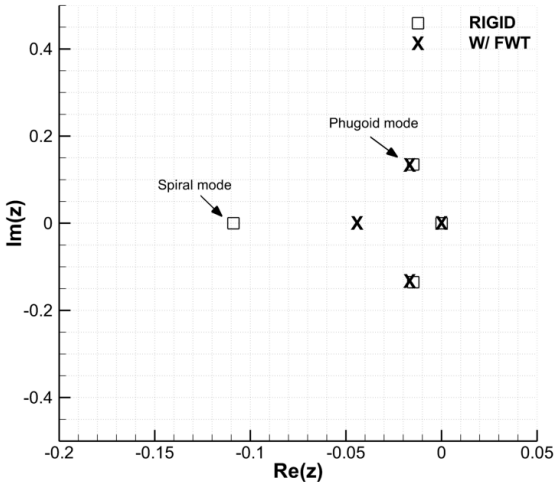

(c) Zoom on region R2

Figure 8: Root locus of flight dynamic modes

value in the negative X direction which leads to an increase in the level of engine operation. However, it has to be remarked that in this study only a simple quasi-steady aerodynamic model which aerodynamically treats the SAH model as three decoupled rigid bodies has been used. These three rigid bodies have definitely some aerodynamic impact on each other and further investigations are needed for conclusive evaluations. Figure 8 provides the root locus of a model linearised around the aforementioned trim conditions for the rigid and SAH aircraft. As can be seen from the figure, by adding the FWTs to the aircraft, some slight changes are reflected on the aircraft flight modes root locus. First, we take a closer look at the longitudinal modes including short-period and phugoid modes. The short-period mode has almost remained unchanged, as the deviation between the rigid and the modified aircraft is quantified to be less than 1%. Although the phugoid mode change is not significant, the rigid aircraft experiences a 10% increase in stability by introducing the SAH concept to the wing. Regarding the lateral modes, i.e. Dutch roll and Spiral modes, from the aspect of stability, the Dutch roll of the SAH aircraft is slightly (around 5%) more stable. The spiral mode underwent the most significant change. By adding the FWTs (each having a mass of about 1 percent of the total aircraft mass) to the rigid aircraft,

the spiral model becomes more unstable by over 60%. From the stability perspective, this may be the most significant change that need to be taken into account in the design of an aircraft including the SAH concept. Once again, we emphasize that a more sophisticated aerodynamic model is needed to perform the stability analysis more accurately.

4 CONCLUSIONS

In this work, the effect of the introduction of FWTs on the representative RCAM model is studied using a multi–body formulation with three decoupled rigid bodies, which allows, with respect to previous work in the literature, to monitor constraint hinge loads and system response in the presence of an initial side-slip angle. The model derivation and implementation is verified by evaluating the state variables, and the fold angle response for different values of FWTs masses and hinge flare angles. From these preliminary results, it was observed that the state variables response is largely affected by increasingly larger FWTs masses, while larger coasting angles are found for correspondingly smaller hinge axis flare angles. It was found from stability analysis of the flight dynamic modes that the modes affected mostly by the introduction of the SAH concept are the spiral modes, with a 60% deviation from the values found for the rigid configuration. Forces and moments acting at the hinges are significant and should be carefully accounted for during the preliminary design stage. For the same trim condition, by adding the folded wing tips of the total mass of 2% of the whole aircraft the engine level operating conditions have been increased by around 10%. This increase in the level of engine operation can be justified by the amount of forces acting at hinges in the opposite of the flight direction. However, further investigations with a more sophisticated aerodynamic model are needed for conclusive evaluations. In the presence of a side-slip angle, the asymmetric transient forces and moments at hinges can lead to larger deviation from the initial flight path. For future work, more accurate aerodynamic models will be integrated (vortex lattice method) and also structural flexibility will be included.

5 ACKNOWLEDGEMENTS

This work was supported by Innovate UK [Grant number 10003388]. We also acknowledge the support from AIRBUS UK.

6 REFERENCES

[1] Mastracci, P., Saltari, F., Mastroddi, F., et al. (2022). Unsteady aeroelastic analysis of the semi aeroelastic hinge including local geometric nonlinearities. *AIAA Journal*, 60, 3147–3165. ISSN 1533385X. doi:10.2514/1.J061108.

[2] Castrichini, A., Siddaramaiah, V. H., Calderon, D. E., et al. (2017). Preliminary investigation of use of flexible folding wing tips for static and dynamic load alleviation. *Aeronautical Journal*, 121, 73–94. ISSN 00019240. doi:10.1017/aer.2016.108.

[3] Wilson, T., Castrichini, A., Azabal, A., et al. (2017). Aeroelastic behaviour of hinged wing tips. *IFASD 2017*.

[4] Ye, B., Yang, Y., and Cheng, Z. (2023). Flare folding wing tips for static and gust loads alleviation. vol. 2459. Institute of Physics. ISSN 17426596. doi:10.1088/1742-6596/2459/1/012071.

[5] Balatti, D., Khodaparast, H. H., Friswell, M. I., et al. (2023). Experimental and numerical investigation of an aircraft wing with hinged wingtip for gust load alleviation. *Journal of Fluids and Structures*, 119. ISSN 10958622. doi:10.1016/j.jfluidstructs.2023.103892.

[6] Castrichini, A., Wilson, T., and Cooper, J. E. (2018). On the dynamic release of the semi aeroelastic wing-tip hinge device. *In: 6th Aircraft Structural Design Conference*.

[7] Leylek, E. A. and Costello, M. (2015). Use of compliant hinges to tailor flight dynamics of unmanned aircraft. *Journal of Aircraft*, 52, 1692–1706. ISSN 15333868. doi:10.2514/1.C033056.

[8] Lambrechts, P. (1995). Robust flight control design challenge problem formulation and manual: the research civil aircraft model. *GARTEUR Open*, 368–381.